Steffen Hein

Large eddy approximation of turbulent flow in DSC schemes

Abstract. Large eddy simulation of turbulent flow is given a natural setting within the DSC framework of computational fluid dynamics. Periodic cellular coarse-graining prevents the nodal flow from piling up and preserves its large patterns. The coarsening operations are consistent with the near-field interaction principle of DSC, and are just as simple in the treatment of boundary conditions. Numerical examples validate the approach.

> L'acte de la nature est simple, et la complexité qu'elle paraît avoir construite
> n'est que l'entrecroisement sans fin des antagonismes qui se sont neutralisés
>
> *Henri Bergson*

1. Introduction

Discrete schemes have to cope with the cursed situation that they first create by breaking space into pieces. Mesh cell systems, however fine, can never be perfect substitute for continuous space. Already in linear algorithms they produce artefacts, such as unphysical *spurious solutions*, and more harmful things happen in the non-linear case.

In fluid dynamics, when the non-linear spectral transfer properties of the Navier-Stokes equations (the *energy cascade*; cf. Pope [Po]) come into play beyond the transition to turbulence, eddies are locally excited, down to very short scale; cf. Kolmogorov [Ko]. Eddies smaller than the cell size cannot be properly resolved by a mesh of realistic coarseness and thus tend to induce local fluctuations that artificially pile up. Large eddy simulation (LES) aims to discard such divergences through regularizing the flow by means of a suitable averaging filter, and to screen its essential *large patterns* in this way.

LES stands for the most promising line in modern turbulence modelling. The name has been coined by Deardorff in 1970, who first applied LES methods to turbulent channel flow [De]. Important elements had yet been kept ready, formerly. Already Reynolds [Re] used temporal flow averages that as *Reynolds averages* play still a rôle in conventional turbulence models. In 1922, Richardson [Ri] proposed mesh cell averages for smoothing down local fluctuations. Such so called *box filters* stand today for one line of LES. Spatial filters of varied type indeed classify modern LES methods. Excellent insight into the state of the art is gained from the recent book of Berselli et al. [BIL], which not only exposes the elaborate mathematical framework but also addresses many items of conventional turbulence modelling (the prominent $k - \epsilon$ model of Launder and Spalding [LS], e.g.).

The present paper differs from most related work in the field in that it sharply separates the natural and technical aspects of turbulent instability and strictly focusses on the latter within the *computational context* in hand. The natural part, viz. essentially (modulo discretization) the Navier-Stokes equations for viscous incompressible flow, are thereby taken as a *physical given*. This is in obvious contrast to widespread use: In many conventional turbulence models, as in some lines of LES, turbulent pile-up is controlled by modifying the underlying dynamic equations or even the physical constants. Such models use, for instance, Reynolds number dependent global parameters - usually an *eddy viscosity*, e.g. - or time and space filtered Navier-Stokes equations or any (e.g. stochastic) variant. All this is allowed, of course, as long as it provides numerical data in harmony with observation. Also, a profound change of the inner dynamics can very efficiently delimit turbulence and thus lead to a convergent scheme. It is yet, obviously, tuning the underlying *physical phenomenon* rather than eliminating the technical cause of divergences that are manifestly an *artefact of discretization*. (Turbulence is still enigmatic in many respects, but *divergence* is certainly not a feature of turbulent flow - observed in the continuum of nature, e.g.) Therefore, the central point of attack in discarding turbulent pile-up will be in this paper the weaknesses of discretization, while the Navier-Stokes equations are directly discretized as taken from physics - which not only combats the desaster at the origin, but also yields validated results.

2. DSC schemes

A mesh cell system is not just poor surrogate continuous space, but it always introduces its proper structure. Cellular meshes, with that we are dealing here, artificially impose local *cell-boundary duality* upon space [He1] - and it is this simple fact that dual scattering channel (DSC) schemes match in a canonical fashion.

DSC schemes are finite volume methods of a very specific type. In technical detail, they are extensively dealt with in [He1], so it is sufficient here to recapitulate their essential features in a crash course like manner. The algorithm is characterized by a two-step cycle of iteration which alternately updates the computed fields within cells and on their interfaces. If the updating instructions are explicit, then a *near-field interaction* principle gives rise to a scattering process interpretation known as *Johns' cycle* [He1]. A pair of vectors that represent the same field within a cell and on its surface essentially constitutes a *scattering channel*. Equivalently, scattering channels are sometimes defined as pairs of distributions that 'measure' the field within a cell and on one of its faces. The well known primal DSC scheme is JOHNS' TLM algorithm, wherein scattering channels are visualised as transmission lines [JoB]. In many applications, such as computational fluid dynamics, the TLM picture of wave propagation fails, but one can still go back to the far more general DSC setup.

Within any *physical interpretation*, cf. [He1], each scattering channel represents a pair of scalar or vector valued distributions $z^p = (\, p \, , \, Z \,)$ and $z^n = (\, p^\sim , \, Z \,)$ which evaluate a physical field Z on the surface and in the interior, respectively, of a mesh cell. A distribution p pertinent to a cell face is called a *port* and $p^\sim$ its *nodal image*, and the two are related by pull-back, viz.

$$(1) \qquad (\, p^\sim , \, Z \,) = (\, p \circ \sigma , \, Z \,) = (\, p \, , \, Z \circ \sigma^{-1} \,) \, ,$$

for every Z (of class C^∞, e.g.), where σ denotes the spatial translation $\sigma : \mathbb{R}^3 \to \mathbb{R}^3$ that shifts the geometric *node* (i.e. the cell centre) in the (centre of) the respective face.

It follows that there exists a *scattering channel representation* of DSC states: If M denotes the mesh cell system, $\partial\zeta$ the boundary of cell $\zeta \in M$ ($\partial\zeta$ is naturally identified with the set of ports with nodal image in ζ), and L_ζ^p the span of the z_ζ^p (i.e. the linear *range* space), then each state in the mesh permits a unique representation in the space

$$(2) \qquad P := \prod_{\zeta \in M} \prod_{p \in \partial\zeta} L_\zeta^p \times L_\zeta^{p^\sim} \, ,$$

with canonical projections $\pi_\zeta^{p,\, n} : P \to P_\zeta^{p,\, n}$ into the port and node components of cell ζ. Furthermore, there is a natural involutary isomorphism $nb : P \to P$,

$$(3) \qquad nb : (\, z^p , \, z^{p^\sim} \,) \mapsto (\, z^{p^\sim} , \, z^p \,) \, ,$$

called the *node-boundary map*, which hence maps P^p onto P^n and vice versa. (The cell index ζ is omitted here and in the following without danger of confusion.)

It stands to reason that the nodal images of different ports (e.g. on different faces of the same cell) can represent the same physical field in a node and may even coincide there as distributions - just as two ports pertinent to neighbouring cells obviously represent the same field on a common face, if they *connect* two channels on it. In fact, the scattering channel representation of DSC states in (2) is in general highly *redundant* - which may be utilized for process parallelization [He1].

Within the algorithm, the port and node components are updated at even and odd integer multiples, respectively, of half a timestep τ and are usually constantly continued as step functions over the subsequent time intervals of length τ.

Note that *existence*, not necessarily explicit *construction* or *application*, of a scattering channel representation characterizes DSC schemes, and that less redundant representations are actually used in many implementations. In fact, the scattering channel representation is basically a theoretical means for describing (and deriving) certain DSC properties - such as the following.

A fundamental principle - closely related to the COURANT-LEVI stability criterion - is *near-field interaction*. It requires that every updated state of a node or face depends only on states (along with their history) in scattering channels *connected* to the respective node or face - the latter *here* being for once identified with its adjacent face, if such exists in any neighbouring cell.

As a consequence of near-field interaction, every DSC process allows for an interpretation as a *multiple scattering process* in the following sense.

Let for any process $z = (z^p, z^n)(t)$ *incident* and *outgoing fields* z^p_{in} and z^n_{out} be recursively defined as processes in P^p and P^n, respectively, by setting $z^p_{in}(t) := z^n_{out}(t - \frac{\tau}{2}) := 0$, for $t < 0$, and for $0 \leq t = m\tau$; $m \in \mathbb{N}$:

(4)
$$z^p_{in}(t) := z^p(t) - nb \circ z^n_{out}(t - \frac{\tau}{2}),$$
$$z^n_{out}(t + \frac{\tau}{2}) := z^n(t + \frac{\tau}{2}) - nb \circ z^p_{in}(t).$$

Then, at every instant holds $z^p(t) = nb \circ z^n_{out}(t - \frac{\tau}{2}) + z^p_{in}(t)$ and $z^n(t + \frac{\tau}{2}) = nb \circ z^p_{in}(t) + z^n_{out}(t + \frac{\tau}{2})$. Also, near-field interaction implies that every state is only a function of states incident (up to present time t) on scattering channels connected to the respective node or face.
More precisely, by induction holds:

Theorem. There exists a pair of functions $\mathcal{R}$ and $\mathcal{C}$, defined on back in time running sequences of incident and outgoing fields, respectively, such that for every cell $\zeta \in M$ the process $z^n_\zeta = \pi^n_\zeta \circ z$ complies with

(5)
$$z^n_\zeta(t + \frac{\tau}{2}) = \mathcal{R}((z^p_{in}(t - \mu\tau))_{p \in \partial\zeta; \mu \in \mathbb{N}})$$

and the port process $z^p_\zeta = \pi^p_\zeta \circ z$ satisfies

(6)
$$z^p_\zeta(t + \tau) = \mathcal{C}((z^n_{out}(t + \frac{\tau}{2} - \mu\tau))_{n \mid \partial\zeta; \mu \in \mathbb{N}}).$$

$\left(\text{'} \mid \text{' short-hand for 'in any of the } (1 \text{ or } 2) \text{ cells adjacent to' } \right)$

Remarks

(i) The statements immediately imply that $z^n_{\zeta, out}$ and $z^p_{\zeta, in}$ are themselves functions of states incident on connected scattering channels, since
$$z^n_{\zeta, out}(t + \frac{\tau}{2}) = \mathcal{R}((z^p_{in}(t - \mu\tau))_{p \in \partial\zeta; \mu \in \mathbb{N}}) - nb \circ z^p_{\zeta, in}(t) \quad \text{and}$$
$$z^p_{\zeta, in}(t) = \mathcal{C}((z^n_{out}(t - \frac{\tau}{2} - \mu\tau))_{n \mid p; \mu \in \mathbb{N}}) +$$
$$- nb \circ z^{p^\sim}_{\zeta, out}(t - \frac{\tau}{2})$$

(ii) $\mathcal{R}$ and $\mathcal{C}$ are called, respectively, the *reflection* and *connection* maps of the DSC algorithm, and a *field excitation* may be implicit in $\mathcal{C}$, cf. [He1].

(iii) Near field interaction implies computational stability, if the reflection and connection maps are α-*passive*, i.e. contractive in this sense [He2].

3. Coarse-graining

Mesh cell systems import artificial defects into space - which yet sometimes carry their remedy in themselves, at least in part: For instance, the cellular mesh, by separating the virtually unresolved cell interior from the coarse-grained cell-boundary *skeleton grid*, necessarily fixes - and hence *delimits* - the scale of local resolution. A clever design always takes into account the coarsening effect of the cellular mesh - which, on the other hand, provides quasi free of charge a basis for large eddy approximation in the DSC setup of computational fluid dynamics. In fact, already intuitively DSC schemes go along with kind of natural large pattern approximation that - in a sense now made precise - associates *cell averages* to some nodal quantities.

The following definition is independent of any particular application and therefore given without reference to fluid dynamics.

Definition (coarse-graining)

For any port $p \in \partial\zeta$ with nodal image $p^\sim$ let B^p denote the set of all ports on $\partial\zeta$, the nodal images of which coincide with $p^\sim$ as distributions. Also, let $w_r \in [0, 1]$; $r \in B^p$, be a set of *weights* such that $\sum_{r \in B^p} w_r = 1$.

Then, every DSC field which in the scattering channel representation on each component $q \in B^p \subset \partial\zeta$ equals $(z^q, z^{q^\sim})$ with

(7)
$$z^{q^\sim} = \sum_{r \in B^p} w_r z^r$$

is named an (*in ζ and with weights w_r*) coarse-grained field (*pertinent to p* - or also *to its nodal image $p^\sim$*).

The nodal state of every such field, coarse-grained in any cell, is hence a convex superposition - i.e. a *weighted mean* - of states that represent the field on the cell surface. Also, substituting a DSC field with any coarse-grained field that (obviously) leaves the cell boundary states unchanged is then called *coarsening this field* (in any component).

   Should such an innocent looking procedure *untie the Gordian knot of turbulence* ? Remember that our modest aim is repairing some defects of discretization - rather than resolving the fundamental questions of turbulence in the way mathematical physics should do that. What matters here is that in the DSC setup of CFD well-timed periodic coarse-graining of the flow efficiently prevents turbulent pile-up, all with retaining the large eddies. Note that the coarsening period should be taken as small as necessary to ensure stability and precision, but large enough against the time step (by one order of magnitude at least - as a rule of thumb): Clearly, coarsening inevitably also interferes with the flow dynamics. However - since the *skeleton field* on the cell boundaries is left unchanged - the perturbation is minimal, and in fact negligible, for suitable periods. Through removing only the turbulent fluctuations of very short range (below a scale given by cell size) which tend to artificially pile-up, coarsening regularises the flow to just such a mild degree that its essential *large* patterns are preserved.

4. Viscous Boussinesq-incompressible flow

The port and node distributions of a DSC algorithm can be *finite integrals* - as is the case for the TLM method, where finite path integrals over electric and magnetic fields are evaluated in a discrete approximation to Maxwell's integral equations [He4-6]. In the case at hand, they are simply *Dirac measures* that pointwise evaluate the fields within the cells and on their surfaces, and composites of Dirac measures which approximate the gradients of these fields; cf. section (5).

   In the *Oberbeck-Boussinesq* approximation [Obb,Bss] all material fluid properties are assumed as constant - *except fluid density which only in the gravitational term varies linearly with temperature*. The energy equation of a *Boussinesq-incompressible* fluid of velocity $\vec{u}$ with thermal diffusivity α, heat source(s) q, and negligible viscous dissipation and heat capacity is then the *convection-diffusion* equation for the temperature T, cf. [GDN],

$$(8) \qquad \frac{\partial T}{\partial t} + div\,(T\,\vec{u}) = \alpha\,\Delta T + q\,.$$

The Navier-Stokes *momentum equations* for (the k-th component of) a Newtonian fluid of dynamic viscosity η, under pressure p, and in a gravitational field of acceleration $\vec{g}$ take the form [e.g. Ptk]

$$(9) \qquad \frac{\partial}{\partial t}\,(\varrho\,\vec{u}_k) + div\,(\varrho\,\vec{u}_k\,\vec{u}) + grad\,p_k = \eta\,\Delta\,\vec{u}_k + \varrho\,\vec{g}_k\,r\,.$$

With $\varrho_\infty = const$ and $\varrho\,(T) = \varrho_\infty\,\beta\,(T\,(t,\vec{x}) - T_\infty)$, wherein $\beta = \varrho^{-1}\,\partial\varrho\,/\,\partial T$, this becomes in the OB-approximation

$$(10) \qquad \frac{\partial\vec{u}_k}{\partial t} + div\,(\vec{u}_k\,\vec{u}) + \frac{grad\,p_k}{\varrho_\infty} = \frac{\eta}{\varrho_\infty}\,\Delta\,\vec{u}_k + \beta\,(T\,(t,\vec{x}) - T_\infty)\,\vec{g}_k\,.$$

Integrating these equations over cell ζ with boundary $\partial\zeta$ and applying Gauss' theorem to integrals over $\Delta = div\,grad$ and $div\,(f\,\vec{u})$ yields with time increment τ the following updating instructions for nodal T and $\vec{u}_k$, these quantities and q being averaged over the cell volume V_ζ

$$(11) \qquad \begin{aligned} T\,(t+\frac{\tau}{2}) &:= T + \\ &+ \frac{\tau}{V_\zeta}\int_{\partial\zeta}(\alpha\,grad\,T - T\,\vec{u})\cdot dS \end{aligned}$$

and

$$(12) \qquad \begin{aligned} \vec{u}_k\,(t+\frac{\tau}{2}) &:= \vec{u}_k + \tau\,(\beta\,(T - T_\infty)\,\vec{g}_k - \frac{grad\,p_k}{\varrho_\infty}) + \\ &+ \frac{\tau}{V_\zeta}\int_{\partial\zeta}(\frac{\eta}{\varrho_\infty}\,grad\,\vec{u}_k - \vec{u}_k\,\vec{u})\cdot dS\,. \end{aligned}$$

In equations (11) and (12) the former updates (at time $t - \tau/2$) of the *nodal* quantities enter the right-hand sides in the *first line*, and the last former updates (at time t) of the *cell face* quantities enter the *second line*.

The nodal values of T and $\vec{u}_k$ are updated at the reflection step - after coarsening the velocity field, e.g. with weights proportional to the pertinent cell face areas, whenever the coarsening period is attained - while the port quantities that enter the surface integrals at the right-hand sides are updated on the connection step of the iteration cycle. The next section outlines how we can proceed with that in a non-orthogonal hexahedral mesh.

5. The non-orthogonal hexahedral cell

The physical interpretation of a DSC algorithm associates a smoothly varying (e.g. in time and space C^∞-) scalar or vector field Z to port and node states z^p and z^n of a mesh cell system.

Let any hexahedral cell be given by its eight vertices. Define then *edge vectors* $({}_\nu e)_{\nu=0,\dots,11}$, *node vectors* $({}_\mu b)_{\mu=0,1,2}$, and *face vectors* $({}_\iota f)_{\iota=0,\dots,5}$, using the labelling scheme of figure 1 a

$$(13) \qquad {}_\mu b := \frac{1}{4} \sum_{\nu=0}^{3} {}_{(4\mu+\nu)} e \qquad\qquad \mu = 0,1,2$$

$$\text{and} \quad {}_\iota f := \frac{(-1)^\iota}{4} \; ({}_{(8+2\iota)} e + {}_{(9+2(\iota+(-1)^\iota))} e) \wedge$$
$$\wedge ({}_{(4+2\iota)} e + {}_{(5+2\iota)} e) \qquad \iota = 0,\dots,5,$$

with all indices understood cyclic modulo 12 and $\wedge$ denoting the cross product in $\mathbb{R}^3$.
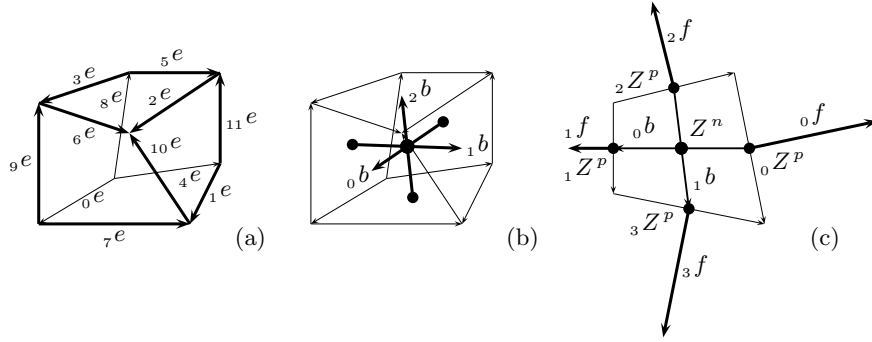

Fig. 1. *Non-orthogonal hexahedral mesh cell.* (a) *Edge vectors.* (b) *Node vectors.* (c) *Face vectors.*

At every cell face $\iota \in \{0,\dots,5\}$ and for any given $\tau \in \mathbb{R}_+$ the following time shifted finite differences of Z in directions ${}_\mu b$ ($\mu = 0,1,2$) form a vector valued function

$$(14) \qquad {}_\iota \nabla^B Z_\mu(t) := \begin{cases} 2(-1)^\iota (Z^n{}_{|t-\tau/2} - {}_\iota Z^p{}_{|t}) & \text{if } \mu = [\iota/2] \\ ({}_{2\mu+1} Z^p - {}_{2\mu} Z^p)_{|t-\tau} & \text{if } \mu \neq [\iota/2] \end{cases}$$

($[x]$ denotes the *integer part* of $x \in \mathbb{R}$). The time increments are chosen conform with the updating conventions of DSC schemes (as will be seen in a moment) and are consistent. In fact, in the first order of the time increment τ and of the linear cell extension, the vector ${}_\iota \nabla^B Z$ in the centre point of face ι approximates the scalar products of the node vectors with the gradient ∇Z. More precisely, let for a fixed centre point on face ι and $\epsilon \in \mathbb{R}_+$ the ϵ-*scaled cell* have edge vectors ${}_\iota e^\sim := \epsilon \, {}_\iota e$. Let also ${}_\iota \nabla^{B\sim} Z_\mu$ denote function (14) for the ϵ-scaled cell (with node vectors ${}_\mu b^\sim = \epsilon \, {}_\mu b$). Then at the fixed point holds

$$(15) \qquad < {}_\mu b, \mathrm{grad}(Z) > = {}_\mu b \cdot \nabla Z = \lim_{\epsilon \to 0} \lim_{\tau \to 0} \frac{1}{\epsilon} {}_\iota \nabla^{B\sim} Z_\mu,$$

as immediately follows from the required C^1-smoothness of the field Z.

To recover the gradient ∇Z from (14) in the same order of approximation, observe that for every orthonormal basis $({}_\nu u)_{\nu=0,\dots,m-1}$ of $\mathbb{R}^m$ or $\mathbb{C}^m$, and for any basis $({}_\mu b)_{\mu=0,\dots,m-1}$ with coordinate matrix $\beta_\nu^\mu = < {}_\nu u, {}_\mu b >$, the scalar products of every vector a with ${}_\mu b$ equal

$$(16) \qquad \underbrace{< {}_\mu b, a >}_{=: \, \alpha_\mu^B} = \sum_{\nu=0}^{m-1} \underbrace{< {}_\mu b, {}_\nu u >}_{(\bar\beta_\mu^\nu) = (\beta_\nu^\mu)^*} \underbrace{< {}_\nu u, a >}_{=: \, \alpha_\nu} = \bar\beta_\mu^\nu \alpha_\nu$$

Note that we observe EINSTEIN's summation convention at the right side of equation (16) and henceforth - but without ever summing over indices appearing as *left-hand* subscripts!

From equation (16) follows

(17) $$\alpha_\nu = \gamma_\nu^\mu \alpha_\mu^B, \qquad \text{with} \qquad (\gamma_\nu^\mu) := ((\beta_\nu^\mu)^*)^{-1} \quad .$$

This applied to the node vector basis $_\mu b$ and (15) yields the approximate gradient of Z at face ι

(18) $$_\iota \nabla Z_\nu \quad = \quad \gamma_\nu^\mu \; _\iota \nabla^B Z_\mu.$$

The scalar product of the gradient with face vector $_\iota f^\nu = \; < \; _\iota f, \, _\nu u >, \; \nu \in \{0, 1, 2\}$, is thus

(19) $$_\iota S \; = \; _\iota f \, \cdot \, _\iota \nabla Z \; = \; \underbrace{_\iota f^\nu \, \gamma_\nu^\mu}_{=: \; _\iota s^\mu} \; _\iota \nabla^B Z_\mu \; = \; _\iota s^\mu \; _\iota \nabla^B Z_\mu \, .$$

Continuity of the gradient at cell interfaces yields linear updating equations for Z^p on the two adjacent faces. In fact, for any two neighbouring cells ζ, χ with common face, labelled ι in cell ζ and κ in χ, continuity requires

(20) $$_\iota^\zeta S \quad = \quad - \, _\kappa^\chi S.$$

Substituting (19) for $_\iota^\zeta S$ and $_\kappa^\chi S$ and observing the time shifts in (14) provides the updating relations for Z^p at the cell interfaces. To make these explicit, we first introduce the quantities $_\iota z_\mu^{p, \, n}$ ($\iota = 0, ..., 5 \, ; \, \mu = 0, 1, 2$)

(21) $$_\iota z_\mu^n (t) \quad := \quad \begin{cases} 2 \, (-1)^\iota \, Z^n \, _{|t} & \text{if } \mu = [\iota/2] \\ (\, _{2\mu+1} Z^p - \, _{2\mu} Z^p \,)_{|t-\tau/2} & \text{else} \end{cases} \quad ,$$

which in virtue of (1) yields $_\iota z_\mu^p = (p, Z) = (p^\sim, Z \circ \, _\iota \sigma^{-1}) =$
$= \, _\iota z_\mu^n \, | \, Z \circ \, _\iota \sigma^{-1}$, where $_\iota \sigma : n \mapsto p$ denotes the nodal shift pertinent to face ι. In particular

(22) $$_\iota z_{[\iota/2]}^p (t) \quad = \quad 2 \, (-1)^\iota \; _\iota Z^p \, _{|t} \, ,$$

which together with (21) is consistent for $\mu \neq [\iota/2]$ with

(23) $$_\iota z_\mu^n (t + \tau/2) \quad = \quad - \frac{1}{2} \, (\, _{2\mu+1} z_\mu^p + \, _{2\mu} z_\mu^p \,) (t) \, .$$

From (14, 19, 21, 22) follows that

(24) $$\begin{aligned} _\iota S \, _{|t+\tau} \quad &= \quad _\iota s^\mu \, (\, _\iota z_\mu^n \, _{|t+\tau/2} - 2 \, (-1)^\iota \delta_\mu^{[\iota/2]} \; _\iota Z^p \, _{|t+\tau}) \\ &= \quad _\iota s^\mu \, (\, _\iota z_\mu^n \, _{|t+\tau/2} - \delta_\mu^{[\iota/2]} \; _\iota z_\mu^p \, _{|t+\tau}) \, . \end{aligned}$$

Continuity of Z, i.e. $_\iota^\zeta Z^p = \, _\kappa^\chi Z^p$, with (20, 21) then implies

(25) $$_\iota^\zeta z_{[\iota/2]}^p (t + \tau) = \frac{_\iota^\zeta s^\mu \; _\iota^\zeta z_\mu^n (t + \tau/2) + \, _\kappa^\chi s^\nu \; _\kappa^\chi z_\nu^n (t + \tau/2)}{_\iota^\zeta s^{[\iota/2]} + (-1)^{\iota + \kappa} \, _\kappa^\chi s^{[\kappa/2]}} \, .$$

For completeness we agree upon setting $_\iota^\zeta z_\mu^p (t + \tau) := \, _\iota^\zeta z_\mu^n (t + \tau/2)$ for $\mu \neq [\iota/2]$ (although this contains a slight inconsistency in that continuity might be infringed; this can easily be remedied by taking the arithmetic mean of the two adjacent values). - In fact, our agreement doesn't do harm, since any discontinuity disappears with mesh refinement.

   We dispose, hence, of a complete set of recurrence relations for z^p (given z^n by the former reflection step) which at the same time determine the field components on face ι and their gradients

(26) $$_\iota \nabla Z_\nu \quad = \quad \gamma_\nu^\mu \; _\iota z_\mu^p.$$

Essentially this constitutes the connection step of the algorithm.
Nodal gradients are similarly (and even more simply) derived, using

$$\nabla^B Z_\mu^n (t + \frac{\tau}{2}) \quad := \quad (\, _{2\mu+1} Z^p - \, _{2\mu} Z^p) (t) \, ; \quad \mu = 0, 1, 2$$

in the place of (14), and then again (18). With the node and cell-boundary values and gradients of T and $\vec{u}$ the nodal updating relations for the latter are immediately extracted from equations (11, 12) in section 4. For equation (11) this is essentially (up to the convective term) carried out in [He1],

section 5, and the procedure remains straightforward in the case at hand. Note that a well-timed LES coarsening routine, cf. section 3, should be periodically carried out before the nodal step of the iteration cycle in order to obviate instablities called forth by the energy cascade [Po].

The updating relations thus obtained are explicit and consistent with near-field interaction (only adjacent quantities enter). So, they can optionally be transformed into scattering relations for incident and reflected quantities (6) along the guidelines of section 2 - with established advantages for stability estimates [He2].

6. Pressure

Unlike compressible flow - wherein a thermodynamic *state equation* relates pressure to density and temperature - Boussinesq-incompressible flow is conserved by pressure acting like a potential against violations of the local flow balance. Hence, the pressure is directly coupled to the flow divergence by *Poisson's equation*:

$$(27) \qquad \Delta p = (\varrho_\infty / \tau) \, div \, \vec{u} .$$

The solution p for fluid velocities updated in the connection step provides a pressure gradient, which in the next reflection step - via equations (10,12) - repairs sporadic violations of the flow balance. Systematic test computations have shown that additional *divergence clearing*, as proposed by the author in earlier papers, e.g. [He3], is not necessary (nor even profitable) - and may be rather on the debit of computational performance and stability.

In integral form, after using Gauss' Theorem, equation (27) becomes

$$(28) \qquad \tau \int_{\partial \zeta} grad \, p \, \cdot \, dF \quad = \quad \varrho_\infty \int_{\partial \zeta} \vec{u} \cdot dF ,$$

which can be solved by a Gauss-Seidel routine or by successive overrelaxation, carried out after updating the face velocities in the connection step.

In each iteration, firstly the discrete cell boundary integral $I_{\partial \zeta} := \int_{\partial \zeta} \vec{u} \cdot dF$ is computed and explicitly - by solving a linear equation in $I_{\partial \zeta}$ and the cellular pressures - the unique p^n that exactly compensates $I_{\partial \zeta}$ so that (28) is satisfied in every cell. In a second run over the mesh, continuity of the pressure gradient is re-established at the cell interfaces by updating the face pressures along the lines of the last section (viz. taking Z as p there). The loop is reiterated until (usually after a few iterations) equations (28) hold with sufficient precision.

7. Conclusion and Completions

The DSC approach to computational fluid dynamics allows for simulation of turbulent flow in a plain and natural way. Cellular coarse-graining efficiently prevents turbulent pile up and preserves the large eddies.

Since the energy cascade starts long before transition to turbulence (actually it is effective over the entire energy spectrum [Po], [BIL, pp. 72 ff.]), a well-timed coarsening routine should escort every DSC fluid flow algorithm. Periodic coarse-graining significantly improves algorithm stability, even in the laminar regime - this without overly altering the flow dynamics, if the coarsening period is chosen as outlined in section 3. Handy criteria for a good choice - in relation to mesh refinement, e.g. - should be subject to further study.

Details of implementation and special applications are clearly beyond the scope of the present study. However, we leave off with some examples for the purpose of illustration.

The graphics displayed have been computed with author's test program DANSE, HEIN [He7], which combines a Maxwell field TLM Solver with a DSC heat transfer and flow algorithm based on this paper.

The computations for coaxial RF power transmission line RL100-230 (with data realistically taken from an ion cyclotron resonance heating experiment in plasma physics) are in excellent keeping with reference computations (FLUENT) and empirical measurements. For a line with inner conductor made of copper and air dielectric at atmospheric pressure the heating process has been simulated in horizontal position from standby to steady state operation with 160 KW transmitted CW power CW power at 100 MHz frequency, with outer conductor cooled at 40 degrees Celsius temperature. Simultaneously, a Maxwell field TLM algorithm run in the same mesh provided the skin effect heat sources.

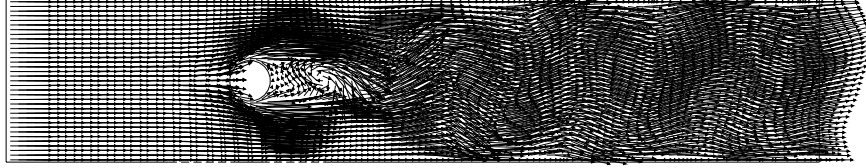**Fig. 2.** *Jet over backward facing step*   *[highly turbulent regime].*

Fig. 3. *Kármán vortex street behind cylinder[snapshot of oscillating flow].*
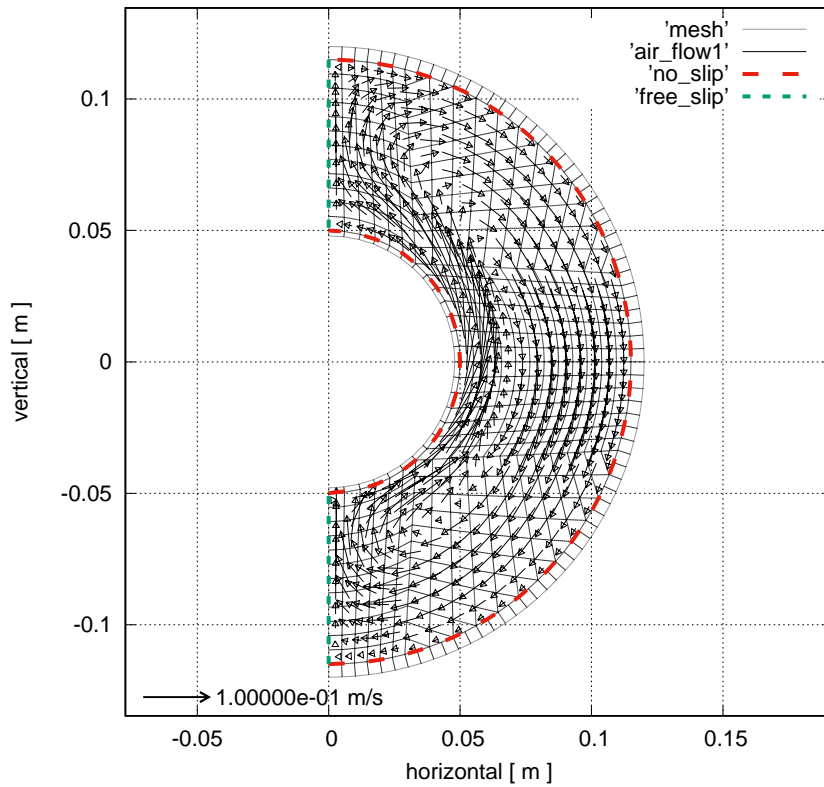

Fig. 4. *Air convection in horizontal coaxial line RL100-230 ;*
transverse section [reference arrow: $0.1\,ms^{-1}$; transmitted power 160 kW CW, frequency 100 MHz; air dielectric; inner conductor copper, outer conductor cooled at 40 degrees Celsius].
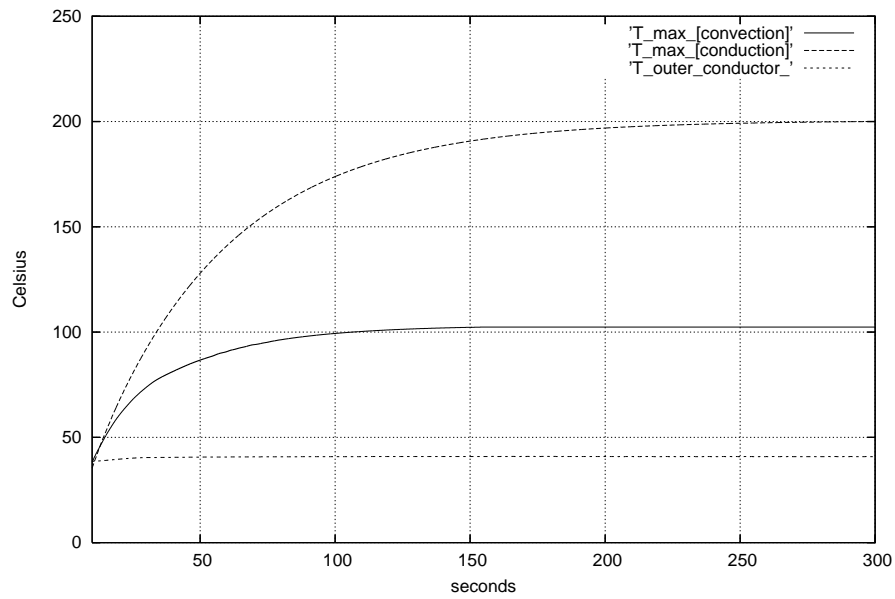
Fig. 5. *Heating process in coaxial line RL100-230 ;*
temperature maximum vs. time from power-on,
convection compared to - fictitious - pure conduction
[transmitted power 160 kW CW, frequency 100 MHz,
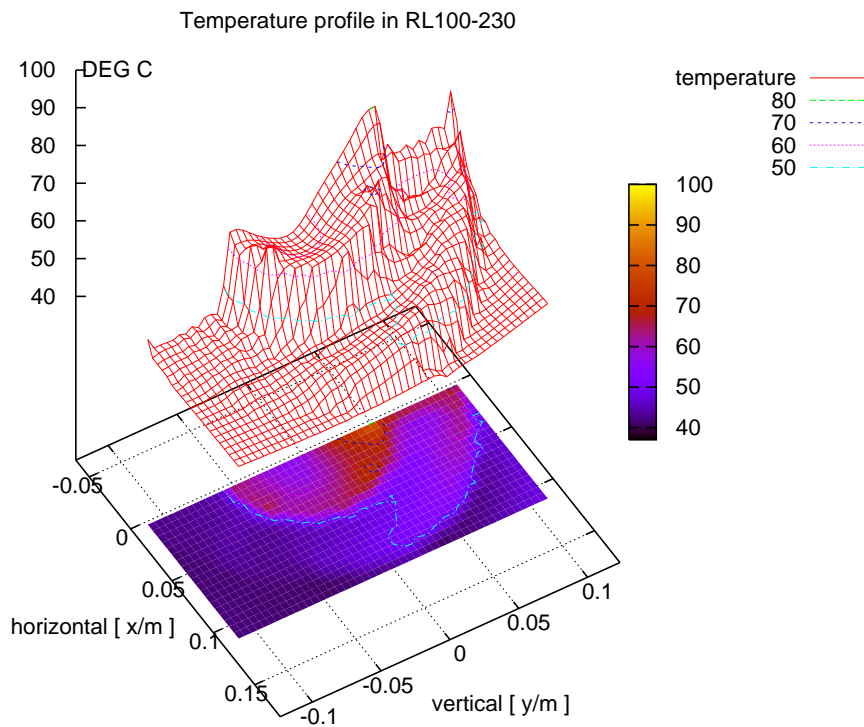*outer conductor cooled at 40 degrees Celsius].*

Fig. 6. *Cross sectional temperature profile in coaxial line RL100-230 computed at steady state [transmitted power 160 kW CW, frequency 100 MHz; air dielectric; inner conductor copper, outer conductor cooled at 40 degrees Celsius].*

References

[Ptk] Ptkankar, S. V., *Numerical Heat Transfer and Fluid Flow*, Taylor and Francis (Hemisphere Publishing Corporation), USA 1980.

[Po] Pope, S. B., *Turbulent flows*, Cambridge University Press, Cambridge 2000.

[Ri] Richardson, L. F., *Weather Prediction by Numerical Process*, Cambridge University Press, Cambridge 1922.

[BIL] Berselli, L. C., Iliescu, T., Layton, W.J., *Mathematics of Large Eddy Simulation of Turbulent Flows*, Springer-Verlag, Berlin Heidelberg, 2006

[LS] Launder, B. E., Spalding, D. B., *Lectures in Mathematical Models of Turbulence*, Academic Press, London 1972

[MS] Meister, A., Struckmeier, J., *Hyperbolic Partial Differential Equations* Theory, Numerics and Applications, Friedrich Vieweg and Sohn, Göttingen 2002

[LMDM] LeVeque, R. J., Mihalas, D., Dorfi, E.A., Müller, E. *Computational Methods for Astrophysical Fluid Flow*, Saas Fee Advanced Courses, 27, Springer-Verlag, Berlin Heidelberg, 1998

[GDN] Griebel, M., Dornseifer, T., Neunhoeffer, T., *Numerical Simulation in Fluid Dynamics*, SIAM monographs on mathematical modeling and computation, Society for Industrial and Applied Mathematics, 1998

[ATP] Anderson, D. A., Tannehill, J. C., Pletcher, R. H., *Computational Fluid Mechanics and Heat Transfer*, series in computaional methods in mechanics and thermal sciences, Hemisphere Publishing Corporation, 1984

[Bss] Boussinesq, J., *Théorie Analytique de la Chaleur*, Gauthiers-Villars, 2., Paris 1903

[Ko] Kolomogorov, A. N., The local structure of turbulence in incompressible viscous fluids for very large Reynolds number. Dokl. Akad. Nauk SSR, vol. 30 (1941), pp. 9-13

[De] Deardorff, J.W., A numerical study of three-dimensional turbulent channel flow at large Reynolds numbers. J. Fluid Mech., vol. 41 (1970), pp. 453-480

[Re] Reynolds, O., On the dynamic theory of the incompressible viscous fluids and the determination of the criterion. Philos. Trans. Roy. Soc. London Ser. A, vol. 186 (1895), pp. 123-164

[Obb] Oberbeck, A., Über die Wärmeleitung der Flüssigkeiten bei Berücksichtigung der Strömung infolge Temperaturdifferenzen., Ann. Phys. Chem., vol. 7 (1879), pp. 271-292

[JoB] Johns, P. B., Beurle R. L., Numerical solution of 2-dimensional scattering problems using transmission line matrix, Proc. IEEE, vol. 118 (1971), pp. 1203-1208

[He1] Hein, S., Dual scattering channel schemes extending the Johns Algorithm, Math. Comp. Simul. vol. 73 (2007) pp. 393-407

[He2] Hein, S., On the stability of dual scattering channel schemes, May 2004, https://arxiv.org/abs/math.NA/0309261

[He3] Hein, S., A DSC approach to Computational Fluid Dynamics, Proceedings of MASCOT 05 - 5th Meeting on Applied Computing and Tools, Lecce - Italy, October 2005, IMACS Series in Computational and Applied Mathematics, vol. 10, pp. 41-50

[He4] Hein, S., Synthesis of TLM Algorithms in the Popagator Integral Framework, Proceedings of the 2nd. Int. Workshop on Transmission Line Matrix Modeling (TLM) - Theory and Applications, pp. 1-11, München, October 1997 (invited paper)

[He5] Hein, S., Finite-difference time-domain approximation of Maxwell's equations with nonorthogonal condensed TLM mesh, Int. J. Num. Modelling, vol. 7 (1994), pp. 179-188

[He6] Hein, S., TLM numerical solution of Bloch's equations for magnetized gyrotropic media, Appl. Math. Modelling, vol. 21 (1997), pp. 221-229

[He7] Hein, S., DANSE - *Discrete Approximation of the Navier Stores Equations for Boussinesq incompressible flow*, April 2007, https://github.com/SteffenHein/danse.gif

Steffen Hein; DE-83043 Bad Aibling, Germany
E-mail address: contact@sfenx.de